AIP | Advances

Tensile strain-induced magnetism transition in multilayer graphene with excess electrons: Stability of the edge-quantum well

Lei Yang and Dongfeng Diao

Citation: AIP Advances **5**, 127106 (2015); doi: 10.1063/1.4937434
View online: http://dx.doi.org/10.1063/1.4937434
View Table of Contents: http://scitation.aip.org/content/aip/journal/adva/5/12?ver=pdfcov
Published by the AIP Publishing

AIP ADVANCES **5**, 127106 (2015)

Tensile strain-induced magnetism transition in multilayer graphene with excess electrons: Stability of the edge-quantum well

Lei Yang[1] and Dongfeng Diao[2,a]
[1]*Key Laboratory of Education Ministry for Modern Design and Rotor-Bearing System, School of Mechanical Engineering, Xi'an Jiaotong University, Xi'an 710049, China*
[2]*Institute of Nanosurface Science and Engineering (INSE), Shenzhen University, Shenzhen 518060, China*

(Received 24 September 2015; accepted 26 November 2015; published online 4 December 2015)

The stability of edge-quantum well-induced strong magnetism of multilayer armchair graphene nanoribbon (AGNR) with excess electrons was investigated under applied tensile strain by density functional theory (DFT) calculations. The results indicated that: (1) The strain along the armchair edge direction led to a transition of the multilayer AGNRs from ferromagnetic state to nonmagnetic state when the strain increased to a critical value; (2) The strain induced bond length changes reduced the stability of the edge-quantum well in terms of the reduction of the electrons capturing capacity; and (3) The spin splitting of the energy bands near the Fermi level reduced with the increase of the strain, resulting in the decrease of the spin moment. This finding suggests that the magnetic properties of graphene have strong dependence on its strain states, which is crucial to the design of graphene-based magnetic devices. [http://dx.doi.org/10.1063/1.4937434]

I. INTRODUCTION

The magnetic properties of graphene based materials have now attracted intensive attentions. Magnetism in graphene has been predicted to be induced by the unique electronic structures localized at topological defects or at special edges.[1–3] In the past few years, a number of experimental works proved the existence of magnetic phenomena in graphene systems. Nair et al. found the magnetism increased with proton irradiation-induced vacancy density by Superconducting Quantum Interference Device (SQUID) measurement.[4] Magda et al.'s Scanning Tunneling Microscopy (STM) test suggested that the magnetic order at the zigzag edge could remain stable at room temperature under a specific crystallographic orientation.[5] Yue et al. developed graphene nanopetals exhibiting robust ferromagnetism with saturation magnetization up to 1.2 emu/g at room temperature.[6] These findings make graphene a promising candidate material for nanoscale magnetic and spintronic devices applications, such as logic transistors and digital memory devices.[7–9]

However, during the manufacturing and the working processes of graphene-based magnetic devices, mechanical strains can be expected to arise either naturally or intentionally.[10–12] For instance, growing graphene on a substrate with different lattice constants can introduce strain.[13,14] The presence of mechanical strain has substantial effect on the electronic structure and magnetic properties of graphene. Zhao et al. studied the effect of uniaxial strain on the magnetism of sawtooth-like graphene nanoribbons (SGNR) and found the ground state of SGNR changes from nonmagnetic state to antiferromagnetic state under uniaxial strain.[15] Choi et al. found the magnetism of Fe/graphene heterostructures was controllable with uniaxial strains.[16] Kou et al. simulated the effect of strain on the magnetic properties of two-dimensional graphene with topological line defects and found that the applied

[a]Corresponding author: dfdiao@szu.edu.cn. Tel: +86-0755-26902415

strain can greatly influence the magnetism of the system.[17] Hu et al. found an external strain-induced transition from a ferromagnetic metal to a ferromagnetic semiconductor in a zigzag-edge graphene nanoribbon with a topological line defect.[18] Moreover, STM results have also proved the effects of strain on the magnetic properties of graphene system.[19,20] These studies suggest that the strain effect on the magnetic properties is extremely important and elucidating the underlying mechanism is crucial to the design of graphene-based magnetic devices.

Our latest research has reported strong magnetism of graphene sheets embedded carbon films at room temperature prepared by electron irradiation assisted physical vapor deposition in electron cyclotron resonance plasma,[21–23] and density functional theory calculations indicate that the magnetism in the graphene nanocrystallines originates from the excess electrons captured by the edge-quantum well in the armchair edges of the graphene nanoribbon.[24] This type of carbon film has potential uses in nanoelectromechanical systems applications, in which mechanical strain may be inevitable, including tensile strain and compressive strain. Therefore, the present work arises from the strain-induced magnetic variations of graphene sheets embedded carbon films. We examined the effects of strain on the stability of the edge-quantum well in multilayer armchair graphene nanoribbon by density functional theory calculations. In this paper, we only studied the tensile strain effect. As for compressive strain, it is believed to enhance the stability of the edge-quantum well, owing to the fact that the edge-quantum well is formed by the contraction of the outermost bond of the armchair graphene nanoribbon (AGNR).

II. METHODS

Multilayer (up to three-layer) AGNR (periodic in the y direction) with a width of 20 atoms (in the x direction) was modeled. The interlayer distance was 0.34 nm. Figure 1(a) shows the top view of a unit cell of monolayer AGNR and Figure 1(b) gives the front view of the multilayer system. A large vacuum slab (at least 1 nm) was added in both the x (ribbon width) and the z (layer stacking) directions. There were 40, 80, and 120 atoms per unit cell for monolayer, bilayer and trilayer AGNR, respectively. The amount of the excess charges, which refers to the excess electrons captured by graphene during electron irradiation, was specified at the beginning of the calculations. In this paper, the amount of the negative excess charges was specified to be two per unit cell, under which the AGNRs were proved to have the highest spin moments according to our earlier study.[24] The red isosurface in Figure 1(a) represents the unpaired spin provided by the excess electrons which would be likely trapped at the edge of the AGNR. External tensile strain was applied along the armchair edge direction (the y direction). The shrinkage along the edge-normal direction (the x direction) due to the Poisson effect was considered with a Poisson's ratio of 0.165.[25]

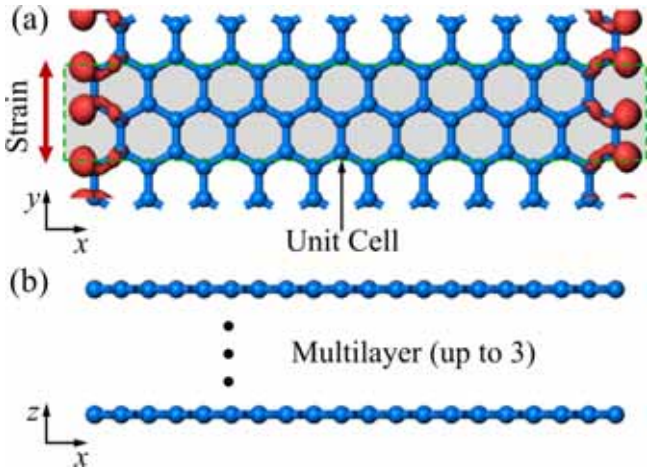

FIG. 1. Schematic illustration of the simulation model, (a) top view of a unit cell of monolayer AGNR, (b) front view of the multilayer AGNRs. The red isosurface represents the unpaired spin provided by the excess electrons which would be likely trapped at the edge of AGNR.

The electronic structures and magnetic properties under different tensile strains were calculated using dispersion-corrected density functional theory (DFT) calculations implemented by the Dmol^3 code.[26] The Perdew-Burke-Ernzerhof (PBE) functional[27] in the generalized gradient approximation (GGA) was employed to describe the exchange-correlation energy. The Tkatchenko-Scheffler scheme[28] of dispersion-correction was chosen to describe the vdW interactions. The all-electron method was used to describe the wave functions with double numeric and polarization basis sets. Spin-unrestricted calculations were performed with both formal spin and manually set spin as initials. The results reported were corresponding to the spin configuration with the lowest total energy. The total energy, electronic structure, and electron densities were solved by the self-consistent field (SCF) method towards the minimum of total energy. Before the energy calculation, geometry optimization was performed to obtain the optimized structure. Other details of the calculations have been introduced in our previous paper.[24]

III. RESULTS AND DISCUSSIONS

Figure 2 shows the total energy (E_{total}, eV) and total spin (μ_{Bohr}) per unit cell of monolayer AGNR as a function of the applied strain along the armchair direction. The total energy without applied strain was set as the reference. As shown in the figure, the total energy increases as a quadratic function of the applied tensile strain, suggesting the applied strain is still in the elastic range of the AGNR, which compares well with Kou et al.'s work.[17] When there is no applied strain, the excess electrons can induce spin moment for all the AGNRs, with a highest value of 1.66 μ_{Bohr} for monolayer AGNR, which is consistent with our previous work. The reason lies in that monolayer graphene has the least coordination number among the three thicknesses. When the tensile strain is applied, for monolayer AGNR, as Figure 2 shows, the spin moment exhibits a slight fluctuation with the increasing of the tensile strain at the early stage. After the strain reaches a value of 9%, further increasing of the tensile strain leads to a sharp decrease of the spin moment. When the strain increases to a critical value of 11%, the spin moment decreases to 0. These results suggest that there is a transition of the AGNR from ferromagnetic state to nonmagnetic state under the applied tensile strain. In order to further clarify the stability of the magnetic state under strain, the energy difference, defined as $\Delta E = E_{Nonmag}$-$E_{Ferromag}$ was calculated. When there is no applied strain, the energy difference is 0.3 eV, indicating that the ferromagnetic state is more stable. However, when strain reaches the critical value, the energy difference decreases to 0 eV, which is consistent with the nonmagnetic state of the AGNR under the critical strain.

Figure 3(a) shows the profiles of Mulliken atomic spin moment along the ribbon width direction and the spin density distributions in the corresponding strain states (0%, 9%, 10%, and 11%) in monolayer AGNR. It is found that the spin distribution is symmetric for both sides from the center along the ribbon width direction and the atomic spin moments are localized at the armchair edge, proving that the magnetism of AGNRs originates from the excess electrons captured by the edge-quantum

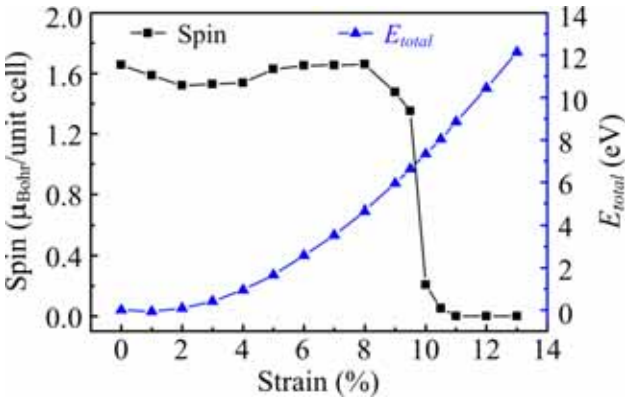

FIG. 2. The total energy and total spin per unit cell of monolayer AGNR as a function of the applied strain.

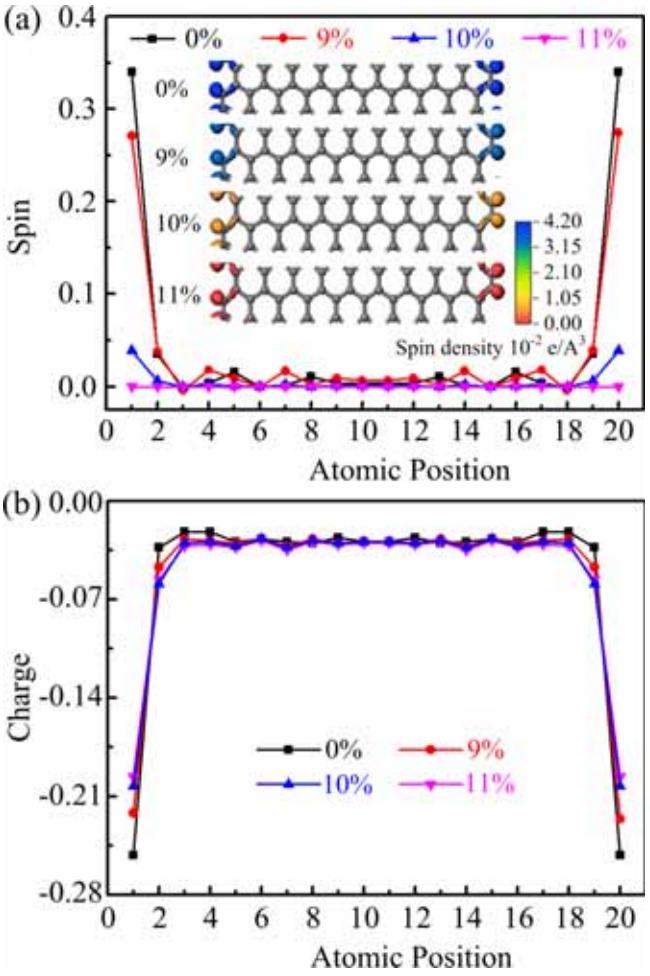

FIG. 3. (a) The profiles of Mulliken atomic spin moment along the ribbon width and the spin density distribution under different strains in monolayer AGNR. (b) The profiles of Mulliken charge along the ribbon width under different strains in monolayer AGNR.

well. As the applied strain increases, the atomic spin moments and spin density localized at the edge sites both decrease. When the strain increases to 11%, the atomic spin moments decrease to 0, which coincides with the decline of the total spin moment under the applied strain, as shown in Figure 2. Figure 3(b) shows the profiles of Mulliken charge along the ribbon width direction in monolayer AGNR under different strains. It can be found that most of the negative charges are localized at the edge atoms. As the strain increases, the value of the negative charges localized at the edge decreases, indicating the applied strain induces a redistribution of the excess electrons.

Figure 4 gives the variations of the total spin (μ_{Bohr}) per unit cell of bilayer and trilayer AGNRs under the applied strain. We can see that the total spin decreases with the increasing of the applied strain for both bilayer and trilayer AGNRs. There is also a transition of the AGNR from ferromagnetic state to nonmagnetic state when the strain increases to a critical value. The critical strain values are 3% and 2% for bilayer and trilayer AGNRs, respectively. Compared with the spin variation of monolayer graphene, it is found that the critical strains for bilayer and trilayer AGNRs are smaller. This is because monolayer AGNR has the best electron capturing capacity since its coordination number is the least. Moreover, according to our previous work,[24] for excess charges e(excess) = −2, the monolayer has the smallest total energy (The E_{total} of e(excess) = 0 is taken as reference for each thickness), suggesting the ferromagnetic state of monolayer AGNR is the most stable. Therefore, the critical strain for the magnetism transition of monolayer AGNR is the largest.

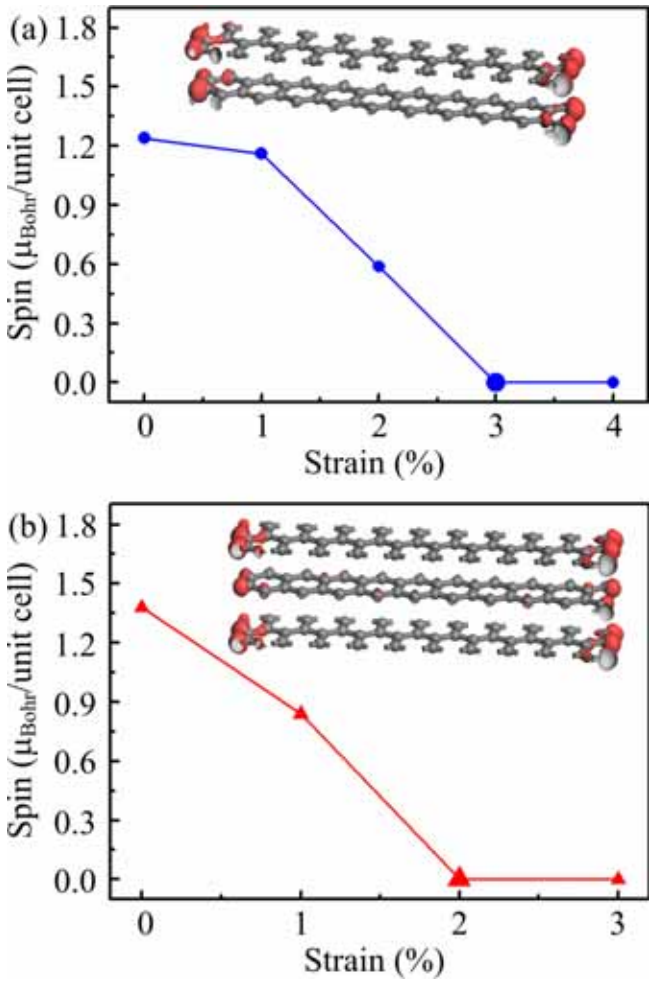

FIG. 4. The total spin (per unit cell) variations under the applied strain in (a) bilayer, and (b) trilayer AGNRs.

As reported previously, the edge-quantum well is formed due to the C-C bond contractions[29,30] at the edge of AGNR induced by under-coordination. Thus the spin moment is closely related to the bond length at the edge of AGNR. When tensile strain is applied, the bond length at the edge of AGNR is altered, which results in variation of the stability of the edge-quantum well. Therefore, in order to interpret the mechanism of the spin moment variation under the applied strain, the bond lengths at the armchair edge of monolayer AGNR under different strains were calculated, Figure 5 shows the local bond length variations at the armchair edge in monolayer AGNR where the atomic spin moments are localized. L_1 and L_2 represent the bond lengths of the outermost and second outermost edge sites. As shown in the figure, when there is no applied strain, L_1 decreases to 0.1301 nm (by -8.38%) while L_2 increases slightly to 0.1421 nm (by 0.07%), compared with the bulk value of 0.1420 nm. As mentioned above, such contraction of the edge bond induces the magnetism of AGNRs. The applied tensile strain brings about the variation of the bond length. When the strain is in the range of 9%, both L_1 and L_2 show fluctuations as the strain increases, which is consistent with the spin moment variation. However, when the strain rises to 10%, L_1 sharply drops while L_2 keeps increasing as the tensile strain increases. This explains the dramatic transition of the magnetism in monolayer AGNR beyond the strain of 10%. It is because such sudden variations of the bond lengths, where the spin moment is localized, could reduce the stability of the edge-quantum well and lead to the redistribution of the excess electrons. Here an interesting point should be noticed, when the strain is in the range of 6% to 10%, the value of L_1 decreases, although it should increase under the tensile strain. The explanation here lies in that there are actually two inverse factors affecting the bond length at

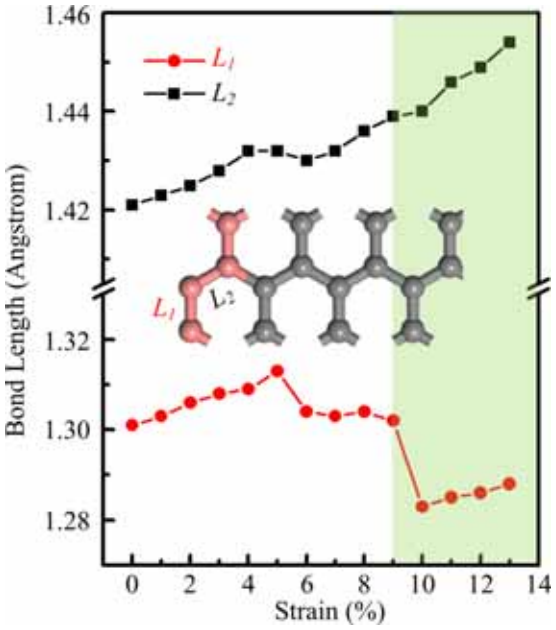

FIG. 5. Bond length variations at the armchair edge of monolayer AGNR as a function of the applied strain. L_1 and L_2 represent the bond lengths of the outermost and second outermost edge sites.

the armchair edge in this study. As is known, the edge quantum well is caused by the spontaneous contraction of the outermost bonds. These bonds tend to elongate when excess electrons are captured by the edge quantum well. For the unstrained monolayer AGNR, L_1 is 0.1237 nm when there are no excess electrons, while it increases to 0.1301 nm with specified excess electrons. When the tensile strain is applied, the outermost bonds are stretched, leading to the reduction of the electrons capturing capacity of the edge-quantum well. As a result, the amount of the trapped electrons at the armchair edge is decreased, which in turn causes the decrease of the bond length at the armchair edge. These two inverse factors are responsible for the bond length variations. For bilayer and trilayer AGNRs, the strain-induced magnetic variations are also related to similar bond length changes at the armchair edges.

For a more comprehensive analysis of the strain effect on the magnetic properties of AGNRs, an analytical model developed by Fujita et al. was used.[31] According to this model, the "damping length" of the edge states is $2\cos(k/2)$. When a strain is applied, the "damping length" should be modified to $2t_2/t_1\ \cos(k/2)$, where t_1 and t_2 are the bond parameters of the AGNR. For tensile strain along the armchair direction, $|t_2/t_1| > 1$, this will slow down the damping of the edge states, leading to the delocalization of such states with reduced electron correlations. Due to electron-electron interaction, the spin polarization at the armchair edge reduces and the spin splitting near the Fermi level decreases. To confirm the above analysis, the spin-polarized band structures of the monolayer AGNR under different strains were calculated, as shown in Figure 6(a) to 6(d). For the band structure computation, the k-path selected was Γ—X. And we employed $3 \times 1 \times 1$ k-point sampling points in the Brillouin zone integration. Figure 6(a) presents the band structure for monolayer AGNR without applied strain. The red and black lines correspond to the spin-up and spin-down bands, respectively. One can see that the spin-up band and spin-down band split into two bands near the Fermi level, suggesting there is a spin splitting band near the Fermi level. This is in accordance with the above calculated ferromagnetic state of monolayer AGNR with excess electrons. When the applied strain increases, the spin splitting is reduced, as shown in Figure 6(b) and 6(c). When the applied strain increases to 11%, the red lines overlaps with the black lines, indicating that the band states near the Fermi level become non-spin-polarized, which coincides with the previously calculated nonmagnetic state of monolayer AGNR with excess electrons under a strain of 11%. Moreover, it can be seen that the spin-up band near the Fermi level rises, while the spin-down band near the Fermi level first rises as

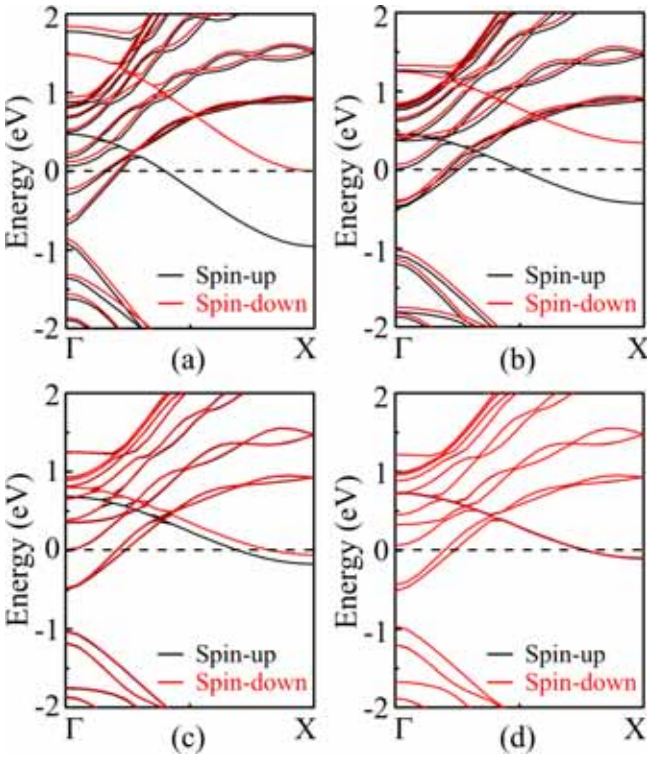

FIG. 6. The spin polarized band structures of the monolayer AGNR in a unit cell under different strains, (a) 0%, (b) 9%, (c) 10%, (d) 11%. The red and black lines correspond to the spin-up and spin-down bands, respectively.

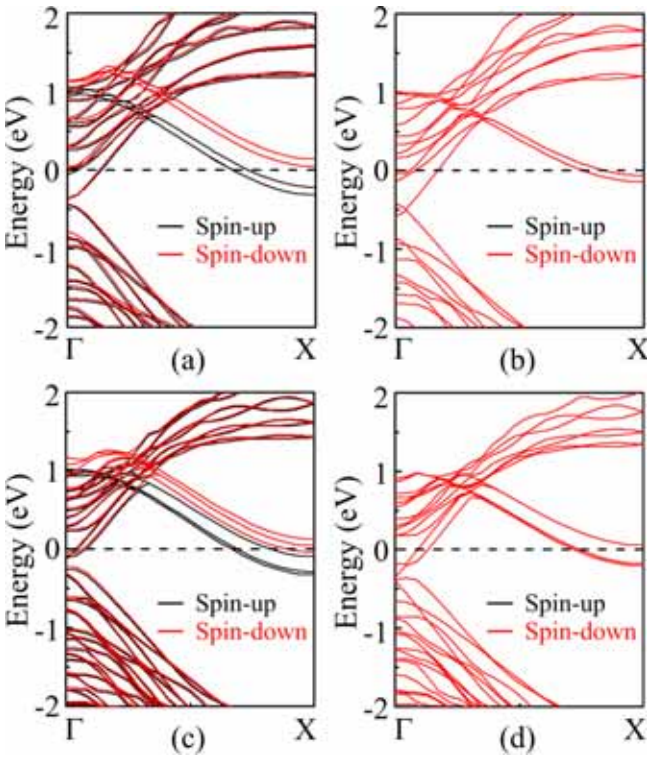

FIG. 7. The spin polarized band structures of the bilayer and trilayer AGNRs in a unit cell under different strains, (a) bilayer 0%; (b) bilayer 3%; (c) trilayer 0%; (d) trilayer 2%.

the strain increases to 9% and then falls as the strain further increases to 10% and 11%. This coincides with the fluctuation of the spin moment when the strain is in the range of 9% (as shown in Figure 2).

The band structures of the bilayer and trilayer AGNRs under different strains were also calculated as shown in Figure 7. As we can see, there is also spin splitting near the Fermi level for both bilayer and trilayer AGNRs without strain. In addition, the spin splitting for bilayer and trilayer AGNRs is smaller than that of monolayer AGNR, which agrees with the magnetism of the three thicknesses of AGNRs. When the strain increased to the critical value, the spin splitting near the Fermi level decreased to 0, as shown in the figure, indicating the AGNRs were in nonmagnetic states under the corresponding strains.

IV. SUMMARY

Density functional theory calculations were performed to elucidate the strain effect on the magnetism of multilayer AGNRs with excess electrons. It was found that there was a transition from ferromagnetic state to nonmagnetic state of AGNR with excess electrons when the tensile strain along the armchair edge direction reached a critical value. For monolayer, bilayer, and trilayer AGNRs with excess charges of -2, the critical strains were 11%, 3%, and 2%, respectively. The strain induced magnetic variations were proved to be related to the bond length changes, which resulted in reduction of the stability of the edge-quantum well. A more comprehensive analysis was conducted to clarify the strain effect based on the band structures of the AGNRs under different applied strains. The results indicated that the applied tensile strain reduced spin polarization at the armchair edges. As a result, the spin splitting near the Fermi level diminished, leading to a decline in the spin moment. This finding suggests that the strain effects should be taken into account when designing graphene-based magnetic devices.

ACKNOWLEDGMENTS

The authors thank the National Nature Science Foundation Major Research Program on Nanomanufacturing under Grant Number of 91323303, the National Nature Science Foundation of China under Grant No. of 51575359, China Postdoctoral Science Foundation under Grant No. of 2015M572547, Research Fund for the Doctoral Program of Higher Education of China under Grant No. of 20120201110029, and the Fundamental Research Funds for the Central Universities.

[1] P. O. Lehtinen, A. S. Foster, Y. C. Ma, A. V. Krasheninnikov, and R. M. Nieminen, Phys. Rev. Lett. **93**, 187202 (2004).
[2] M. M. Ugeda, I. Brihuega, F. Guinea, and J.M. Gomez-Rodriguez, Phys. Rev. Lett. **104**, 096804 (2010).
[3] Z. S. L. Lei, B. Li, E. Kan, J. Huang, Q. X. Li, and J. T. Yang, J. Appl. Phys. **113**, 213709 (2013).
[4] R. R. Nair, I-L Tsai, M. Sepioni, O. Lehtinen, J. Keinonen, A. V. Krasheninnikov, A. H. C. Neto, M. I. Katsnelson, A. K. Geim, and I. V. Grigorieva, Nat. Commun. **4**, 2010 (2013).
[5] G. Z. Magda, X. Z. Jin, I. Hagymasi, P. Vancso, Z. Osvath, P. N. Incze, C. Y. Hwang, L. P. Biro, and L. Tapaszto, Nature **514**, 608 (2014).
[6] Z. J. Yue, D. H. Seo, K. Ostrikov, and X. L. Wang, Appl. Phys. Lett. **104**, 092417 (2014).
[7] K. S. Novoselov, V. I. Fal'ko, L. Colombo, P. R. Gellert, M. G. Schwab, and K. Kim, Nature **490**, 192 (2012).
[8] S. Entani, H. Naramoto, and S. Sakai, J. Appl. Phys. **117**, 17A334 (2015).
[9] T. Kato, T. Nakamura, J. Kamijyo, T. Kobayashi, Y. Yagi, and J. Haruyama, Appl. Phys. Lett. **104**, 252410 (2014).
[10] Z. H. Ni, T. Yu, Y. H. Wang, Y. Y. Wang, Y. P. Feng, and Z. X. Shen, ACS Nano **2**, 2301 (2008).
[11] T. M. G. Mohiuddin, A. Lombardo, R. R. Nair, A. Bonetti, G. Savini, R. Jalil, N. Bonini, D. M. Basko, C. Galiotis, N. Marzari, K. S. Novoselov, A. K. Geim, and A. C. Ferrari, Phys. Rev. B **79**, 205433 (2009).
[12] G. V. Troppenz, M. A. Gluba, M. Kraft, J. Rappich, and N. H. Nickel, J. Appl. Phys. **114**, 214312 (2013).
[13] N. Ferralis, R. Maboudian, and C. Carraro, Phys. Rev. Lett. **101**, 156801 (2008).
[14] J. Borysiuk, R. Bozek, W. Strupinski, A. Wysmolek, K. Grodecki, R. Steapniewski, and J. M. Baranowski, J. Appl. Phys. **105**, 023503 (2009).
[15] S. Q. Zhao, Y. Lu, Y. C. Zhang, W. G. Lu, and W. J. Liang, Appl. Phys. Lett. **104**, 203105 (2014).
[16] H. Choi, E. W. Lee, S. B. Cho, and Y. C. Chung, J. Appl. Phys. **111**, 07C306 (2012).
[17] L. Z. Kou, C. Tang, W. L. Guo, and C. F. Chen, ACS Nano **5**, 1012 (2011).
[18] T. Hu, J. Zhou, J. M. Dong, and Y. Kawazoe, Phys. Rev. B **86**, 125420 (2012).
[19] N. Levy, S. A. Burke, K. L. Meaker, M. Panlasigui, A. Zettl, F. Guinea, A. H. Castro Neto, and M. F. Crommie, Science **329**, 544 (2010).
[20] N.-C. Yeh, M.-L. Teague, S. Yeom, B. L. Standley, R. T.-P. Wu, D. A. Boyd, and M. W. Bockrath, Surface Science **605**, 1649 (2011).

[21] C. Wang, D. F. Diao, X. Fan, and C. Chen, Appl. Phys. Lett. **100**, 231909 (2012).
[22] C. Wang and D. F. Diao, Appl. Phys. Lett. **102**, 052402 (2013).
[23] C. Wang, X. Zhang, and D. F. Diao, Nanoscale **7**, 4475-4481 (2015).
[24] X. Zhang, C. Wang, C. Q. Sun, and D. F. Diao, Appl. Phys. Lett. **105**, 042402 (2014).
[25] M. Mohr, K. Papagelis, J. Maultzsch, and C. Thomsen, Phys. Rev. B **80**, 205410 (2009).
[26] B. Delley, J. Chem. Phys. **92**, 508–517 (1990).
[27] J. P. Perdew, K. Burke, and M. Ernzerhof, Phys. Rev. Lett. **77**, 3865 (1996).
[28] A. Tkatchenko and M. Scheffler, Phys. Rev. Lett. **102**, 073005 (2009).
[29] X. Zhang, J.-L. Kuo, M. Gu, P. Bai, and C. Q. Sun, Nanoscale **2**, 2160–2163 (2010).
[30] C. Q. Sun, Prog. Mater. Sci. **54**, 179–307 (2009).
[31] M. Fujita, K. Wakabayashi, and K. Nakada, J. Phys. Soc. Jpn. **65**, 1920–1923 (1996).